Investigation on grain refinement mechanism of Ni-based coating with LaAlO$_3$ by first-principles

Xuebing Zhao [a],JiZhang [b], Sha Liu [a],Changchun Zhao [a], Caixia Wang [a], Xuejun Ren [c], Qingxiang Yang [a,]

[a]State Key Laboratory of Metastable Materials Science and Technology, Yanshan University, Qinhuangdao 066004, China b College of Mechanical Engineering, Yanshan University, Qinhuangdao 066004, China.

[b]School of Engineering, Liverpool John Moores University, Liverpool L3 3AF, UK

In this work, the adhesion energy, interfacial energy, interface bonding and interface magnetism of LaAlO3/Ni interface were calculated by the first-principles method. Meanwhile, the effectiveness of LaAlO3 as the heterogeneous nucleus of Ni grains was also analyzed. The results show that the Wad of the AlO2-O-OT interface is the largest, which is 3.58 J/m2. Those of the LaO-OT interface and AlO2-Al-OT interface are followed. While that of the LaO-MT interface is the smallest. Interface magnetism analysis shows that the AlO2-terminated interface en¬hances the polarization of Ni atom, and the LaO-OT interface has a little influence on the polarization of Ni atom, while the LaO-MT interface reduces the polarization of Ni atom. The LaO-terminated interface is more stable than the AlO2-terminated interface when ΔμAl is low. While the AlO2-terminated interface becomes more stable when ΔμAl is high. When ΔμAl is less than −14.15 eV and −11.74 eV, the interfacial energy of the LaO-MT interface and LaO-OT interface is smaller than the liquid/solid interfacial energy of Ni (σNi(l)/Ni(s)). When ΔμAl is more than −9.09 eV and −6.63 eV, the interfacial energy of the AlO2-O-OT and AlO2-Al-OT interfaces is smaller than σNi(l)/Ni(s). Therefore, LaAlO3 can be the heterogeneous nucleus of Ni and refine Ni grains.

1. Introduction

With excellent wear resistance, high-temperature oxidation and corrosion resistance, Ni-based alloy (such as NiCrBSi, Ni + WC) coatings were widely applied in mineral processing, oil exploration, cement and steel industries [1–4]. By adding hard phases into the Ni-based alloy coatings, the hardness and wear resistance of the coatings were increased simultaneously [5,6]. However, with the existence of hard phases, the toughness of the coatings was decreased. Therefore, it is significant to increase the toughness, and ensure the hardness and wear resistance of the Ni-based coatings [1,7,8].

By adding rare earth (RE) oxides (such as CeO2,La2O3), the mechanical property, corrosion resistance and oxidation resistance of the Nibased alloy coatings are improved [9,10]. Many researches [7–13] have reported the effect of RE oxides (CeO2,La2O3)additives on the microstructure and mechanical property of the Ni-based coatings. S.P. Sharma [7] studied the influence of La2O3 on the microstructure, hardness and wear behavior of flame sprayed Ni based coatings, and found that the La2O3 additive can refine the grain size, and improve wear resistance of the coatings. Parisa Farahmand [8] investigated the corrosion and wear behavior of laser cladded Ni-WC coatings with the addition of La2O3. The result showed that when an optimal addition of La2O3 is 1 wt.%, the grain size of Ni binder is refined and the corrosion resistance and wear resistance of the coatings can be improved. Z.Y. Zhang [11] researched the effect of CeO2 on the microstructure and wear behavior of thermal spray welded NiCrWRE coatings, and indicated that the hardness and wear resistance of the coatings are significantly increased by the CeO2 additive. However, the grain refinement mechanism of Ni-based coating has been rarely reported by experiment.

Currently, the first-principles calculation based on density functional theory (DFT) as an important microscopic study method has been widely used in modern science. It can not only analyze detailed atomic and electronic structures of the interface, but also calculate the interfacial adhesion work and interfacial energy, which is crucial to deeply explain the phenomena of heterogeneous nucleation [14–17]. Especially, the adhesion work and interfacial energy can reflect the binding strength and interfacial stability of the interface, which affects the heterogeneous nucleation rate directly. Han [14] calculated the interface properties of Al/TiB2 interface by the first-principles method, and indicated the theoretical mechanism of TiB2 as heterogeneous nucleation of Al grains. J. Yang [15] calculated the interface adhesive energy, interfacial energy, electronic structure and bonding of austenite/LaAlO3 interface, and proved that LaAlO3 can be the heterogeneous nucleus of austenite and refine austenite grains. H.L. Zhang [16] investigated the structural properties of the liquid/solid interface between TiB2 substrate and Al melt during heterogeneous nucleation by first-principles calculations. K. Li [17] calculated the interface properties of Mg/Al4C3 interface, and analyzed the effectiveness of Al4C3 as the heterogeneous nucleus of Mg grains. Therefore, in this work, the grain refinement mechanism of Ni-based coating with La2O3 additive will be investigated by the first-principles method.

In the molten pool with RE oxide La2O3 additive, there are many chemical reactions existing at high temperature. La2O3 will transform into various La inclusions by reacting with the impurity elements Al, O and S, which indicates that La2O3 can play a role for deoxidizing and desulfuring [9,18]. Our group's prophase research [19] indicated that, in various La inclusions, the formation free energy of LaAlO3 is the minimum, which proves that LaAlO3 is formed in the melt pool preferentially. Therefore, in the Ni-based coating with La2O3 additive, whether the La inclusion LaAlO3 can be the heterogeneous nucleus of Ni and refine Ni grains will be investigated in this work. In the present study, the interface adhesion energy, interfacial energy, interface bonding and interface magnetism of polar LaAlO3(100)/ Ni(100) interface were calculated by using first-principles method, which can provide theoretical basis for LaAlO3 as the heterogeneous nucleus of Ni grains.

2. Calculation method

All calculations in this work were performed by first-principles method based on density functional theory (DFT), as implemented in the Cambridge serial total energy package (CASTEP) code. The ultrasoft pseudopotentials were employed to represent the interactions between valence electrons and ionic core. Generalized gradient approximation (GGA) of Perdew-Burke-Ernzerhof (PBE) approach was applied to describe the exchange-correlation functional [20]. Because d and f electrons exist in La atom, the strong correlation effect must be considered, in which Hubbard U was employed. The kinetic energy cut-off value [21] of 370 eV was used for plane wave expansions. The k-point sampling grids obtained by using Monkhorst-Pack method [22] were set to 8 × 8 × 8 for bulk LaAlO3 and Ni, 7 × 7 × 1 for all the slabs.

Surfaces and interfaces were modeled with periodic boundary conditions. Before the interface was constructed, convergence tests of LaAlO3 and Ni slabs were done to determine the minimum atomic layers for meeting bulk-like interiors. A vacuum layer of 15 Å was selected for each surface and interface structure in order to eliminate the interactions between surface atoms. The Broyden-Fletcher-Goldfarb-Shannon (BFGS) [23,24] algorithm was applied to relax the models to reach the optimized structures. The energy change during the optimization finally converged to less than 1.0×10^{-5} eV/atom. The maximum force was 0.03 eV/Å, and the maximum displacement was 1.0×10^{-3} Å.

3. Results and discussion

3.1. Bulk and surface properties

3.1.1. Bulk properties of LaAlO3 and Ni

In order to assess the accuracy of the computation methods, a series of calculations on the bulk LaAlO3 and Ni were performed firstly. The calculated optimum lattice constant of bulk LaAlO3 is α = 3.837 Å, which is in well agreement with the experimental value (α =3.828 Å [25]) and other reported results (α = 3.839 Å [18], α =3.807 Å [26]). For bulk Ni, the calculated optimum lattice constant is α = 3.536 Å, which is also in line with the experimental data (α =3.52 Å [27])and those from literatures (α =3.540 Å [28], α =3.517 Å [29]). The spin-polarized calculations show that the magnetic moment of bulk Ni (fcc) is 0.60 μB, which is consistent with the results reported in other literatures [29,30]. The above results indicate that the computation methods are accurate enough to guarantee the reliability of the following calculations.

3.1.2. Surface properties of LaAlO3 and Ni

Before the interface is constructed, it is crucial to ensure that both sides of the interface are sufficiently thick to show bulk-like interiors. To determine the minimum atomic layers for meeting bulk-like interiors, convergence tests of LaAlO3 (100) and Ni (100) slabs were done firstly. Ni (100) surface is non-polar surface. The surface energy of Ni (100) surface can be given by [31]:

$$\sigma = \frac{1}{2A}\left(E_{slab}^{N} - N\Delta E\right) \tag{1}$$

$$\Delta E = \left(E_{slab}^{N} - E_{slab}^{N-2}\right)/2 \tag{2}$$

where N is the atomic layers of the slabs; LaAlO3 (100) surface is polar surface. According to the terminated types of atoms, it can be divided into AlO2-terminated and LaO-terminated surfaces. The surface energy of LaAlO3 (100) surface under Alrich and O-rich condition can be given by:

$$\sigma = \frac{1}{2A}\left[E_{\mathrm{slab}} - n_{\mathrm{La}}\mu_{\mathrm{LaAlO_3}}^{\mathrm{bulk}} + (n_{\mathrm{La}} - n_{\mathrm{Al}})\mu_{\mathrm{Al}}^{\mathrm{bulk}} + (3n_{\mathrm{La}} - n_{\mathrm{O}})\mu_{\mathrm{O}}^{\mathrm{bulk}}\right] \tag{3}$$

Surface energy of LaAlO3 (100) and Ni (100) surfaces as a function of atomic layers is listed in Table 1. Fromit, surface energy of Ni (100) surface converges rapidly to 2.34 J/m2 for a 7 atom-layers slab, which is in well agreement with the experimental value 2.38 J/m2 by Ref. [32]. For LaAlO3 (100) surface, the AlO2-terminated surface and LaO-terminated surface converge to −3.44 J/m2 and 7.36 J/m2 when the atomic layers $n \geq 7$, respectively. Besides, the changes of interlayer distance in percent of bulk interlayer spacing of LaAlO3 (100) surface after full relaxation were also analyzed. It is found that the atomic relaxations are mainly concentrated in the top three layers. When the atomic layers $n \geq 7$, the changes of the top two layers (⊿12) of AlO2-terminated surface and LaO-terminated surface converge to −3.2% and +1.0%, respectively, and the slab interiors can reach bulk-like characteristics basically. The results are in linewith Ref. [18]. Therefore, according to the convergence tests, 7-layer atomstructures of LaAlO3 and Ni are selectedwhen the interface structures are built, as shown in Fig. 1. Actually, surface stability of compounds varies with different terminated types of atoms. Because of the non-stoichiometric characteristics of LaAlO3 (100) surface, chemical potentials of different elements need to be considered when the surface energy is calculated. The surface energy of LaAlO3 (100) surface can be given by [33,34]:

$$\sigma = \frac{1}{2A}\left[E_{\mathrm{slab}} - n_{\mathrm{La}}\mu_{\mathrm{La}} - n_{\mathrm{Al}}\mu_{\mathrm{Al}} - n_{\mathrm{O}}\mu_{\mathrm{O}}\right] \tag{4}$$

where Eslab is the total energy of the surface structure; A is the surface area; nLa, nAl and nO are the numbers of La, Al and O atoms in the slabs; µLa, µAl and µO are the chemical potentials of corresponding atoms, respectively. After full relaxation, the surface structure will tend to an equilibrium state. Its chemical potential is equivalent to its bulk one. Therefore, the following relationships exist:

$$\mu_{\mathrm{LaAlO_3}}^{\mathrm{bulk}} = \mu_{\mathrm{La}} + \mu_{\mathrm{Al}} + 3\mu_{\mathrm{O}} \tag{5}$$

$$\Delta H_{\mathrm{LaAlO_3}} = \mu_{\mathrm{LaAlO_3}}^{\mathrm{bulk}} - \mu_{\mathrm{La}}^{\mathrm{bulk}} - \mu_{\mathrm{Al}}^{\mathrm{bulk}} - 3\mu_{\mathrm{O}}^{\mathrm{bulk}} \tag{6}$$

where µLaAlO3 bulk is the total energy of bulk LaAlO3;µLa bulk, µAl bulk and µO bulk are the total energy of La, Al and O atoms in the pure metal La, Al and oxygen, respectively; ΔHLaAlO3 is the heat of formation of bulk LaAlO3, which is taken to be −17.89 eV/unit in this study. Combining Eq. (4) with Eq. (5), µLa can be eliminated to obtain the following equation:

$$\sigma = \frac{1}{2A}\left[E_{\mathrm{slab}} - n_{\mathrm{La}}\mu_{\mathrm{LaAlO_3}}^{\mathrm{bulk}} + (n_{\mathrm{La}} - n_{\mathrm{Al}})\mu_{\mathrm{Al}} + (3n_{\mathrm{La}} - n_{\mathrm{O}})\mu_{\mathrm{O}}\right] \tag{7}$$

Because the actual condition is O-rich condition, µO is equal to1/2 µbulk O2 With the relationship of
ΔµAl=µAl−µAl
bulk, Eq. (7) becomes:

$$\sigma = \frac{1}{2A}\left[E_{\mathrm{slab}} - n_{\mathrm{La}}\mu_{\mathrm{LaAlO_3}}^{\mathrm{bulk}} + (n_{\mathrm{La}} - n_{\mathrm{Al}})\mu_{\mathrm{Al}}^{\mathrm{bulk}} + \frac{1}{2}(3n_{\mathrm{La}} - n_{\mathrm{O}})\mu_{\mathrm{O_2}}^{\mathrm{bulk}} + (n_{\mathrm{La}} - n_{\mathrm{Al}})\Delta\mu_{\mathrm{Al}}\right]$$

In addition, the chemical potentials of La, Al and O atoms in the slabs must be smaller than those in their bulk phases, or the slabs would be unstable to decompose into the elemental phases immediately. Therefore, the following equation can be given:

Combined with Eqs. (5), (6), (9), the minimum and maximum
values of ΔµAl can be given

$$\Delta\mu_{\mathrm{i}} = \mu_{\mathrm{i}} - \mu_{\mathrm{i}}^{\mathrm{bulk}} \leq 0 (i = \mathrm{La, Al, O}) \tag{9}$$

Combined with Eqs. (5), (6), (9), the minimum and maximum values of ΔµAl can be given by:

$$\Delta H_{\mathrm{LaAlO_3}} \leq \Delta\mu_{\mathrm{Al}} \leq 0 \tag{10}$$

The surface energy of LaAlO3 (100) surface as a function of Al chemical potential (ΔµAl) is shown in Fig. 2. Fromit,with the increase of ΔµAl, the surface energy of LaO-terminated surface increases gradually, while that of AlO2-terminated one decreases. When ΔµAl is low, the surface energy of LaO-terminated surface is lower than that of the AlO2-terminated one,which indicates that it ismore stable than the latter. However, when ΔµAl is high, the surface energy of AlO2-terminated surface is lower than that of LaO-terminated one, which indicates that the AlO2- terminated surface becomes more stable.

3.2. Interface properties between LaAlO3 and Ni

3.2.1. Interface geometry

According to the results of convergence tests, the LaAlO3/Ni interface model was built with a 1 × 1 superlattice geometry, in which a 7-layer LaAlO3 (100) slab and a 7-layer Ni (100) slab are combined with the orientation relationship: LaAlO3[011]//Ni[011] and LaAlO3(100)//Ni(100). The lattice mismatch (δ) between LaAlO3 and Ni was calculated by Bramfitt planar lattice misfit formula [35], as listed in Table 2. From it, the mismatch between LaAlO3 surface and Ni surface is 8.5%, which indicates that the interface between LaAlO3 and Ni is a semi-coherent interface. Therefore, the coherent interface approximation is invoked to accommodate the periodic boundary conditions, in which the softer Ni is stretched to match the dimensions of

LaAlO3. In addition to considering different types of terminations, the stacking sequences of interfacial atoms were taken into account when the interface model is built. In this work, there are two stacking sequences: OT and MT. For the AlO2-terminated interface, Al-OT indicates that the interfacial Ni atoms of Ni side are located on the top of Al atom and vacancy in the surface of LaAlO3 side. O-OT represents that the Ni atoms of Ni side are placed on the top of O atoms in the surface of LaAlO3 side. For the LaO-terminated interface, OT indicates that the interfacial Ni atoms of Ni side reside directly on the top of La atom and O atom in the surface of LaAlO3 side. MT represents that the Ni atoms of Ni side are located on top of the middle of surface atoms of LaAlO3 side. The model geometry of LaAlO3(100)/Ni(100) interface is shown in Fig. 3.

3.2.2. Interface adhesion

Binding strength of the interface can be judged by thework of adhesion (Wad), which is defined as the reversible work when an interface is separated into two free surfaces. Wad of the interface can be given by [14,15,36–37]:

$$W_{ad} = E_{LaAlO_3} + E_{Ni} - E_{LaAlO_3/Ni} \tag{11}$$

where ELaAlO3 and ENi are the total energy of LaAlO3 slab and Ni slab, respectively; ELaAlO3/Ni is the total energy of the interface system; A is the interface area. Beforewe relaxed the LaAlO3/Ni interfacemodel, the initial interface separation d0 was set to be 1.919 Å, which is equal to the interlayer distance of LaAlO3 substrate. After full relaxation of the interface model, the interface separation d0 can be obtained from the distance of interfacial atoms of LaAlO3 side and Ni side. The optimal Wad and d0 values for the relaxed geometries of the four LaAlO3/Ni interfaces are listed in Table 3. From Table 3, theWad of the four LaAlO3/Ni interfaces exhibits the following sequence: AlO2-O-OT interface N LaO-OT interface N AlO2-Al-OT interface N LaO-MT interface. It is obvious that the AlO2-O-OT interface exhibits the largest Wad (3.58 J/m2) and the smallest interfacial separation d0 (2.046 Å), which indicates that the binding of the AlO2-O-OT interface is the strongest in all the interfaces. The Wad of the LaO-OT interface follows, which is 3.07 J/m2. While the LaO-MT interface exhibits the smallest Wad (1.76 J/m2), as well as the largest d0 (2.461 Å). These may all be related with the bonding type of the interfacial atoms.

3.2.3. Interface stability

Generally, the lower the interfacial energy is, themore stable the interface is. The interfacial energy γ can be given by Ref. [38,39]:

$$\gamma = \sigma_{LaAlO_3} + \sigma_{Ni} - W_{ad} \tag{12}$$

where σLaAlO3 and σNi are the surface energy of LaAlO3 (100) and Ni (100) surfaces, respectively; Wad is the work of adhesion of LaAlO3/Ni interface. The interfacial energy as a function of ΔμAl for the four LaAlO3/Ni interfaces is shown in Fig. 4, in which the level dotted line is the liquid/ solid interfacial energy of Ni (σNi(l)/Ni(s)). From Fig. 4, when ΔμAl is low, the interfacial energy of LaO-terminated interfaces is lower than that of the AlO2-terminated ones, which indicates that the LaO-terminated interface is more stable than the latter. With the increase of ΔμAl, the interfacial energy of AlO2-terminated interfaces decreases gradually, while that of LaO-terminated ones increases. When ΔμAl is high, the interface stabilities overturn, in which the interfacial energy of AlO2-terminated interfaces is lower than that of the LaO-terminated ones,which indicates that the AlO2-terminated interface becomes more stable. Besides, for the AlO2-terminated interface, in the entire range of ΔμAl, the interfacial energy of AlO2-O-OT interface is lower than that of the AlO2-Al-OT interface, which indicates that it is more stable than the latter.While for the LaO-terminated interface, the interfacial energy of LaO-OT interface is lower than that of the LaO-MT interface, which indicates that the LaO-OT interface is more stable. The results are in line with the above analysis results of Wad.

3.2.4. Electronic structure and bonding

The binding of interfacial atoms depends on the electronic structure and bonding of the interface, which can be discussed by charge density, charge density difference and Mulliken population analysis in this work.

3.2.4. Electronic structure and bonding
The binding of interfacial atoms depends on the electronic structure and bonding of the interface, which can be discussed by charge density, charge density difference and Mulliken population analysis in this work. The charge density difference can be given by:

$$\Delta\rho = \rho_{\mathrm{total}} - \rho_{\mathrm{LaAlO_3(100)}} - \rho_{\mathrm{Ni(100)}} \qquad (13)$$

where ρtotal is the self-consistent charge density of the total LaAlO3/Ni interface system; ρLaAlO3(100) and ρNi(100) are the non-self-consistent charge densities of isolated LaAlO3 (100) slab and Ni (100) slab, respectively. The charge density distributions and the charge density differences for the LaAlO3/Ni interfaces are shown in Figs. 5 and 6, respectively. It is obvious that chemical bonds are formed between interfacial atoms of LaAlO3 side and Ni side in all the interfaces, while the bonding strength is different. From Fig. 5(a), a relatively weak chemical bond is formed in the AlO2-Al-OT interface. In Fig. 6(a), a wide range of charge depletion region exists in the interfacial Al atom. The lost charge transfers to the interface and mixes with that from the Ni atom of Ni side, which proves the formation of covalent/metallic bond. For the LaO-OT interface, in Fig. 5(b), the charge accumulation between the interfacial O atom and Ni atom indicates that the covalent bond with considerable strength is formed at the interface. While the charge accumulation between the interfacial La atom and Ni atom indicates the formation of metallic/covalent bond. From Fig. 6(b), charge depletion region exists in the interfacial Ni atom of Ni side, and charge accumulation region exists in the interfacial O atom of LaAlO3 side, which proves that the ionic bond is formed between interfacial Ni atom and O atom. While the charge accumulation between the interfacial La atom and Ni atom proves the point of Fig. 5(b) once again. For the AlO2-O-OT interface, in Fig. 5(c), the obvious charge accumulation between the interfacial O atom and Ni atom indicates the formation of strong covalent bond. Its interfacial separation is relatively small. From Fig. 6(c), awide range of charge depletion region exists in the interfacial Ni atom. The lost charge transfers to the O atom of LaAlO3 side, which indicates that a polar covalent bond is formed in the interface. This partly explains the reason that the AlO2-O-OT interface exhibits the largest Wad. For the LaO-MT interface, Figs. 5(d) and 6(d) both indicate that the chemical bond formed in the interface is not obvious, which explains the reason that the LaO-MT interface exhibits the smallest Wad and the largest d0. To further clarify the bonding characteristics of the LaAlO3/Ni interfaces, the Mulliken bond population was analyzed, as listed in Table 4.

From Table 4, for the AlO2-Al-OT interface, the overlap population of Al-Ni(Al-OT) bond is 0.29, which indicates that the covalent bond is formed between interfacial Al atom and Ni atom.While the population of O-Ni(MT) bond is 0.15,which indicates the formation of a weak covalent bond between interfacial O atom and MT-Ni atom. Combined with the above analysis results of charge density and charge density difference, the bonding of the AlO2-Al-OT interface is mainly covalent. For the LaO-OT interface, the bond overlap population of La-Ni(La-OT) bond is −1.04. From the point of view of molecular orbital theory, it can be explained as the electrostatic repulsion between charged La atom and Ni atom, which suggests the formation of metallic bond between La and Ni atoms [40]. The population of O-Ni(O-OT) bond is 0.22, which indicates the formation of covalent bond between interfacial O atom and Ni atom. Therefore, the bonding of the LaO-OT interface is a mixture of covalent bond, ionic bond and metallic bond. For the AlO2-O-OT interface, the overlap population of Al\\Ni bond is 0.18, which indicates the formation of covalent bond. However, the O\\Ni bond exhibits the largest population (0.46) and the smallest bond length (1.970 Å), which proves that the strong covalent bond is formed between interfacial O atom and Ni atom. Therefore, the bonding of the AlO2-O-OT interface is covalent and ionic.

3.2.5. Interface magnetism

The Spin-polarized partial DOS for atoms of the four LaAlO3/Ni interfaces and the bulk Ni are shown in Fig. 7(a–e). Fromthem, the Ni PDOSs of the four interfaces are strongly different from that of the bulk one, while all Ni atoms are in ferromagnetic state in all the structures. The calculated up and down DOSs of interfacial O, Al and La atoms are almost symmetric, which indicates that these atoms are weakly polarized and their magnetic moments are negligible. The spin magnetic moments for various Ni atoms are shown in Fig. 7(f). Generally, the larger the magnetic moment is, the stronger the exchange force is, which can result in the shorter bond length and the larger bond energy [41].

For the AlO2-Al-OT interface, the spin magnetic moments of Al-OT Ni atom and MT Ni atom are 0.68 μB and 0.96 μB, respectively. They are both larger than that of the bulk Ni,which is 0.60 μB.While the magnetic moment of Ni atom of the AlO2-O-OT interface is 0.76 μB, which is also larger than that of the bulk one. These results indicate that the formation of AlO2-terminated interface enhances the polarization of Ni atom. For the LaO-OT interface, the magnetic moments of O-OT Ni atom and La-OT Ni atom are 0.68 μB and 0.42 μB, respectively. The average value is 0.55 μB, which differs slightly from that of the bulk Ni. However, the magnetic moment of Ni atom of the LaO-MT interface is 0.32 μB, which is far less than that of the bulk Ni. This indicates that the formation of LaO-MT interface reduces the polarization of Ni atom.

3.3. Heterogeneous nucleation analysis of Ni/LaAlO3

S.P. Sharma [7] investigated the influence of La2O3 additive on the microstructure and wear behavior of NiCrBSi coatings, and proved that the La2O3 additive can refine the grain size of Ni binder, as shown in Fig. 8. Bramfitt misfit theory [35] indicates that, during heterogeneous nucleation, the nucleus with δ b 6% is the most effective, and the nucleus with 6% b δ b 12% is medium effective, while the nucleus with δ N 12% is ineffective. According to the orientation relationship in this work, the mismatch between LaAlO3 (100) surface and Ni (100) surface is 8.5%, which proves that LaAlO3 as the heterogeneous nucleus of Ni is medium effective. During the solidification, to make LaAlO3 as the heterogeneous nucleus of Ni, the interfacial energy of LaAlO3/Ni interface must be smaller than the liquid/solid interfacial energy of Ni, which is 0.265 J/m2 [42], as shown by the level dotted line in Fig. 4. FromFig. 4, in the most range of ΔμAl, the interfacial energy of LaAlO3/Ni interfaces is smaller than that between primary Ni phase and Ni melt (σNi(l)/Ni(s)). Specifically, when ΔμAl is less than −14.15 eV and −11.74 eV, the interfacial energy of the LaO-MT interface and LaO-OT interface is smaller than 0.265 J/m2, respectively. When ΔμAl is more than −9.09 eV and −6.63 eV, the interfacial energy of the AlO2-O-OT and AlO2-Al-OT interfaces is smaller than 0.265 J/m2, respectively. On these conditions, LaAlO3 can be the heterogeneous nucleus of Ni and refine Ni grains. Moreover, although the calculations in this work were performed at 0 K, it has been confirmed that temperature has little influence on the interface stability [43]. Therefore, the calculated results at 0 K are credible to analyze the related experimental interfaces at high temperature.

4. Conclusions

The interface adhesion energy, interfacial energy, interface bonding and interface magnetism of LaAlO3/Ni interface were calculated by the first-principles method in this work, which aimed at analyzing the effectiveness of LaAlO3 as the heterogeneous nucleus of Ni grains. Four interface structures of AlO2-Al-OT, AlO2-O-OT, LaO-OT and LaO-MT were taken into account in this work. The conclusions are given as follows:

(1)When the atomic layers n ≥ 7, both LaAlO3 (100) slab and Ni (100) slab reach bulk-like characteristics basically. For LaAlO3 (100) surface, when ΔμAl is low, the LaO-terminated surface is more stable AlO2-terminated surface becomes more stable. (2) For the four LaAlO3/Ni interfaces, the Wad of the AlO2-O-OT interface is the largest, which is 3.58 J/m2. Those of the LaO-OT interface and AlO2-Al-OT interface are followed, which are 3.07 J/m2 and 2.24 J/m2, respectively. While that of the LaO-MT interface is the smallest, which is 1.76 J/m2. The charge density, charge density difference and Mulliken population analysis indicate that, the bonding of the AlO2-Al-OT interface ismainly covalent, and that of the LaO-OT interface is a mixture of covalent bond, ionic bond and metallic bond, while that of the AlO2-O-OT interface is covalent and ionic. (3) Interface magnetism analysis indicates that, for the AlO2-Al-OT and AlO2-O-OT interfaces, the spin magnetic moments of Ni atoms are both larger than that of the bulk Ni. It indicates that the formation of AlO2-terminated interface enhances the polarization of Ni atom. For the LaO-OT interface, the magnetic moment of Ni atom differs slightly from that of the bulk Ni. However, the magnetic moment of Ni atom of the LaO-MT interface is far less than that of the bulk Ni, which indicates that the formation of LaO-MT interface reduces the polarization of Ni atom. (4) When ΔμAl is low, the LaO-terminated interface is more stable than the AlO2-terminated interface.When ΔμAl is high, the AlO2-terminated interface becomes more stable. Besides, for the AlO2-terminated interface, the AlO2-O-OT interface is more stable than the AlO2-Al-OT one. While for the LaO-terminated interface, the LaO-OT interface is more stable. (5) For the four LaAlO3/Ni interfaces, when ΔμAl is less than −14.15 eV and −11.74 eV, the interfacial energy of the LaO-MT interface and LaO-OT interface is smaller than the liquid/solid interfacial energy of Ni (σNi(l)/Ni(s)), respectively. When ΔμAl is more than −9.09 eV and −6.63 eV, the interfacial energy of the AlO2-O-OT and AlO2-Al-OT interfaces is smaller than σNi(l)/Ni(s), respectively. Therefore, LaAlO3 can be the heterogeneous nucleus of Ni and refine Ni grains.

Acknowledgments

The authors acknowledge financial support by the National Natural Science Foundation of China under the Contract Nos. 51271163 and 51471148, and the Hebei Province Basic Research Foundation of China under the Contract No. 16961008D.

References

[1] Q.S. Ma, Y.J. Li, J. Wang, K. Liu, Microstructure evolution and growth control of ceramic particles in wide-band laser clad Ni60/WC composite coatings, Mater. Des. 92 (2016) 897–905.
[2] Z.K. Weng, A.H. Wang, X.H. Wu, Y.Y. Wang, Z.X. Yang, Wear resistance of diode laser-clad Ni/WC composite coatings at different temperatures, Surf. Coat. Technol. 304 (2016) 283–292.
[3] K. Liu, Y.J. Li, J.Wang, In-situ reactive fabrication and effect of phosphorus on microstructure evolution of Ni/Ni\\Al intermetallic composite coating by laser cladding, Mater. Des. 105 (2016) 171–178.
[4] Z. Shafiee, M.E. Bahrololoom, B. Hashemi, Electrodeposition of nanocrystalline Ni/ Ni-Al2O3 nanocomposite modulated multilayer coatings, Mater. Des. 108 (2016) 19–26.
[5] T. Liyanage, G. Fisher, A.P. Gerlich, Microstructures and abrasive wear performance of PTAW deposited Ni-WC overlays using different Ni-alloy chemistries, Wear 274-275 (2012) 345–354.
[6] L. Benea, S.B. Basa, E. Danaila, N. Caron, O. Raquet, P. Ponthiaux, J.P. Celis, Fretting and wear behaviors of Ni/nano-WC composite coatings in dry and wet conditions, Mater. Des. 65 (2015) 550–558.
[7] S.P. Sharma, D.K. Dwivedi, P.K. Jain, Effect of La2O3 addition on the microstructure, hardness and abrasive wear behavior of flame sprayed Ni based coatings, Wear 267 (2009) 853–859.
[8] P. Farahmand, R. Kovacevic, Corrosion and wear behavior of laser cladded Ni-WC coatings, Surf. Coat. Technol. 276 (2015) 121–135.
[9] K.L. Wang, Q.B. Zhang, M.L. Sun, X.G. Wei, Y.M. Zhu, Rare earth elements modification of laser clad nickel based alloy coatings, Appl. Surf. Sci. 174 (2001) 191–200.
[10] K.L. Wang, Q.B. Zhang, M.L. Sun, X.G. Wei, Y.M. Zhu, Microstructure and corrosion resistance of laser clad coatings with rare earth elements, Corros. Sci. 43 (2001) 255–267.
[11] Z.Y. Zhang, Z.P. Wang, B.N. Liang, H.B. Dong, S.V. Hainsworth, Effect of CeO2 on the microstructure and wear behavior of thermal spray welded NiCrWRE coatings, Wear 262 (2007) 562–567.
[12] T. Zhao, X. Cai, S.X.Wang, S.A. Zheng, Effect of CeO2 onmicrostructure and corrosive

wear behavior of laser-cladded Ni/WC coating, Thin Solid Films 379 (2000) 128–132.
[13] Z. Zhang, Z. Wang, B. Liang, Tribological properties of flame sprayed Fe-Ni-RE alloy coatings under reciprocating sliding, Tribol. Int. 39 (2006) 1462–1468.
[14] Y.F. Han, Y.B. Dai, D. Shu, J. Wang, B.D. Sun, First-principles calculations on the stability of Al/TiB2 interface, Appl. Phys. Lett. 89 (2006) 144107.
[15] J. Yang, P.F. Zhang, Y.F. Zhou, X.L. Xing, X.J. Ren, Y.L. Yang, Q.X. Yang, Mechanical properties of the hardfacing alloys with different La2O3 additives and the mechanism analysis by first-principles calculations, Mater. Sci. Eng. A 591 (2014) 82–89.
[16] H.L. Zhang, Y.F. Han, Y.B. Dai, J. Wang, B.D. Sun, An ab initio molecular dynamics study: liquid-Al/solid-TiB2 interfacial structure during heterogeneous nucleation, J. Phys. D. Appl. Phys. 45 (2012) 455307.
[17] K. Li, Z.G. Sun, F.Wang, N.G. Zhou, X.W. Hu, First-principles calculations onMg/Al4C3 interfaces, Appl. Surf. Sci. 270 (2013) 584–589.
[18] J. Yang, J.H. Huang, D.Y. Fan, S.H. Chen, X.K. Zhao, LaAlO3 as the heterogeneous nucleus of ferrite: experimental investigation and theoretical calculation, J. Alloys Compd. 683 (2016) 357–369.
[19] Y.F. Zhou, Y.L. Yang, X.W. Qi, Y.W. Jiang, J. Yang, X.J. Ren, Q.X. Yang, Influence of La2O3 addition on microstructure and wear resistance of Fe\\Cr\\C cladding formed by arc surface welding, J. Rare Earths 30 (2012) 1069–1074.
[20] J.P. Perdew, K. Burke, M. Ernzerhof, Generalized gradient approximation made simple, Phys. Rev. Lett. 77 (1996) 3865–3868.
[21] N. Troullier, J.L. Martins, Efficient pseudopotentials for plane-wave calculations, Phys. Rev. B 43 (1991) 1993–2006.
[22] H.J. Monkhorst, J.D. Pack, Special points for Brillouin-zone integrations, Phys. Rev. B 13 (1976) 5188–5192.
[23] T.H. Fischer, J. Almlof, General methods for geometry and wave function optimization, J. Phys. Chem. 96 (1992) 9768–9774.
[24] B.G. Pfrommer,M. Côté, S.G. Louie, M.L. Cohen, Relaxation of crystals with the quasi-Newton method, J. Comput. Phys. 131 (1997) 133–140.
[25] B.C. Chakoumakos, D.G. Schlom, M. Urbanik, J. Luine, Thermal expansion of LaAlO3 and (La,Sr)(Al,Ta)O3, substrate materials for superconducting thin-film device applications, J. Appl. Phys. 83 (1998) 1979–1982.
[26] X. Luo, B. Wang, Y. Zheng, First-principles study on energetics of intrinsic point defects in LaAlO3, Phys. Rev. B 80 (2009) 104115.
[27] C. Kittel, Introduction to Solid State Physics, Wiley Interscience, New York, 1986.
[28] Y. Wang, Z.K. Liu, L.Q. Chen, Thermodynamic properties of Al, Ni, NiAl, and Ni3Al from first-principles calculations, Acta Mater. 52 (2004) 2665–2671.
[29] R.S. Dutta, A. Arya, C. Yusufali, B. Vishwanadh, R. Tewari, G.K. Dey, Formation of aluminides on Ni-based superalloy 690 substrate, their characterization and firstprinciple Ni(111)/NiAl(110) interface simulations, Surf. Coat. Technol. 235 (2013) 741–747.
[30] A. Ernst, G. van der Laan,W.M. Temmerman, S.S. Dhesi, Z. Szotek, Contesting results for magnetic moments in nickel thin films, Phys. Rev. B 62 (2000) 9543.
[31] J. Boettger, Nonconvergence of surface energies obtained from thin-film calculations, Phys. Rev. B 49 (1994) 16798–16800.
[32] W.R. Tyson,W.A. Miller, Surface free energies of solid metals: estimation from liquid surface tension measurements, Surf. Sci. 62 (1977) 267–276.
[33] X.G.Wang, A. Chaka,M. Scheffler, Effect of the environment on α-Al2O3 (0001) surface structures, Phys. Rev. Lett. 84 (2000) 3650–3653.
[34] J. Li, M. Zhang, Y. Zhou, G.X. Chen, First-principles study of Al/A13Ti heterogeneous

nucleation interface, Appl. Surf. Sci. 307 (2014) 593–600.
[35] B.L. Bramfitt, The effect of carbide and nitride additions on the heterogeneous nucleation behavior of liquid iron, Metall. Mater. Trans. B Process Metall. Mater. Process. Sci. 1 (1970) 1987–1995.
[36] J. Guo, L.G. Liu, S. Liu, Y.F. Zhou, X.W. Qi, X.J. Ren, Q.X. Yang, Stability of eutectic carbide in Fe-Cr-Mo-W-V-C alloy by first-principles calculation, Mater. Des. 106 (2016) 355–362.
[37] Y.J. Xian, R.Z. Qiu, X. Wang, P.C. Zhang, Interfacial properties and electron structure of Al/B4C interface: A first-principles study, J. Nucl. Mater. 478 (2016) 227–235.
[38] J.R. Smith, W. Zhang, Stoichiometric interfaces of Al and Ag with Al2O3, Acta Mater. 48 (2000) 4395–4403.
[39] M. Christensen, S. Dudiy, G. Wahnström, First-principles simulations of metal-ceramic interface adhesion: Co/WC versus Co/TiC, Phys. Rev. B 65 (2002) 045408.
[40] Y.F. Li, Y.M. Gao, B. Xiao, T. Min, S.Q. Ma, D. Yi, Theoretical calculations on the adhesion, stability, electronic structure, and bonding of Fe/WC interface, Appl. Surf. Sci. 257 (2011) 5671–5678.
[41] J.H. van der Merwe, Interfacial energy: bicrystals of semi-infinite crystals, Surf. Sci. 67 (2001) 365–381.
[42] V.P. Skripov, in: E. Kaldis, H. Scheel (Eds.),Crystal Growth andMaterials, 1977 North-Holland, Amsterdam.
[43] W. Zhang, J.R. Smith, A.G. Evans, The connection between ab initio calculations and interface adhesion measurements on metal/oxide systems: Ni/Al2O3 and Cu/Al2O3, Acta Mater. 50 (2002) 3803–3816.

Table 1
Surface energy of $LaAlO_3$ (100) and Ni (100) surfaces.

	Surface energy (J/m^2)		
	Ni (100)	$LaAlO_3$ (100)	
Layers, n		AlO_2-termination	LaO-termination
3	2.52	−3.33	7.47
5	2.40	−3.39	7.42
7	2.34	−3.44	7.36
9	2.32	−3.43	7.36
11	2.33	−3.44	7.37

Table 2
Planar lattice misfit between $LaAlO_3$ and Ni.

Matching interface	$(100)_{LaAlO3}//(100)_{Ni}$		
$[uvw]_{LaAlO3}$	[010]	[011]	[001]
$[uvw]_{Ni}$	[010]	[011]	[001]
θ	0	0	0
d_{LaAlO3} (Å)	3.838	5.428	3.838
d_{Ni} (Å)	3.536	5.000	3.536
δ (%)	8.5		

Table 3
Interface ideal adhesion energy Wad and interfacial separation d_0 for the four $LaAlO_3$/Ni interface systems.

		Relaxed	
Termination	Stacking	d_0/Å	$W_{ad}/J\ m^{-2}$
AlO_2	Al-OT	2.192	2.24
	O-OT	2.046	3.58
LaO	OT	2.348	3.07
	MT	2.461	1.76

Table 4

Mulliken bond population analysis results between the interfacial atoms for the $LaAlO_3$/Ni interfaces. OT is on top of the interfacial atom. MT is on top of the middle of interfacial atoms.

Termination	Stacking	Bond	Length (Å)	Population
AlO_2	Al-OT	Al—Ni(Al—OT)	2.511	0.29
		O—Ni(Al—OT)	2.893	−0.08
		O—Ni(MT)	2.541	0.15
	O-OT	Al—Ni	2.786	0.18
		O—Ni	1.970	0.46
LaO	OT	La—Ni(La—OT)	2.628	−1.04
		O—Ni(O—OT)	2.098	0.22
	MT	La—Ni[a]	–	–
		O—Ni[a]	–	–

[a] The atomic distance is too long to form a chemical bond.

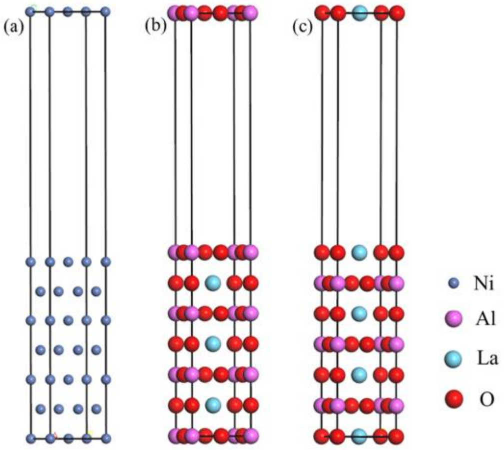

Fig. 1. Crystal Structures of Ni (100) slab and LaAlO3 (100) slab with 7-layer atoms. (a) Ni, (b) AlO2-terminated LaAlO3, (c) LaO-terminated LaAlO3.

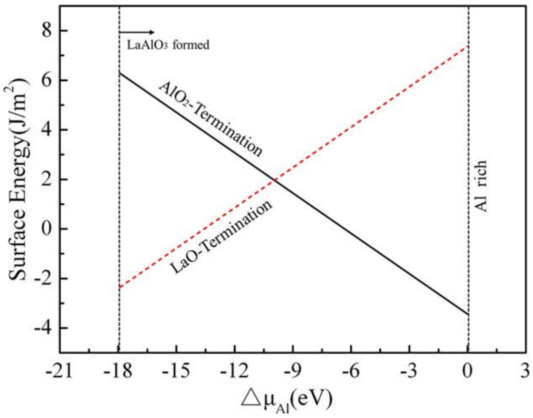

Fig. 2. Surface energy of LaAlO3 (100) surface as a function of ΔμAl.

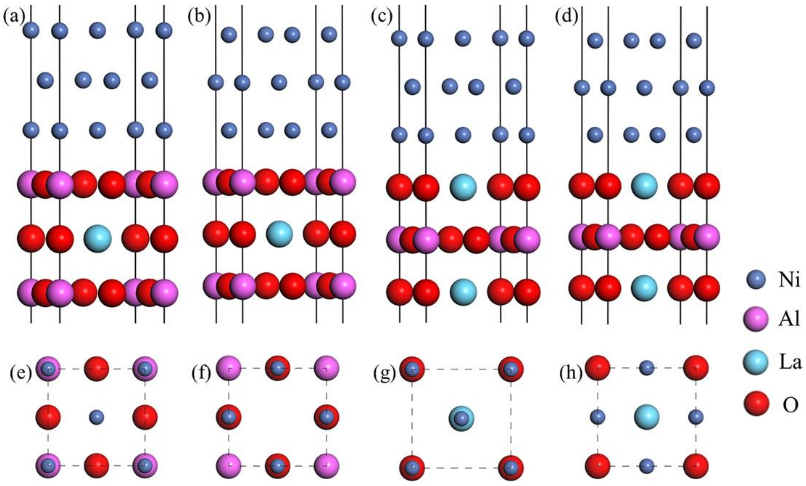

Fig. 3. Crystal Structures of LaAlO3(100)/Ni(100) interfaces. (a) AlO2-Al-OT interface, (b) AlO2-O-OT interface, (c) LaO-OT interface, (d) LaO-MT interface. (e), (f), (g) and (h) are top views of the interfacial atoms corresponding to (a), (b), (c) and (d), respectively.

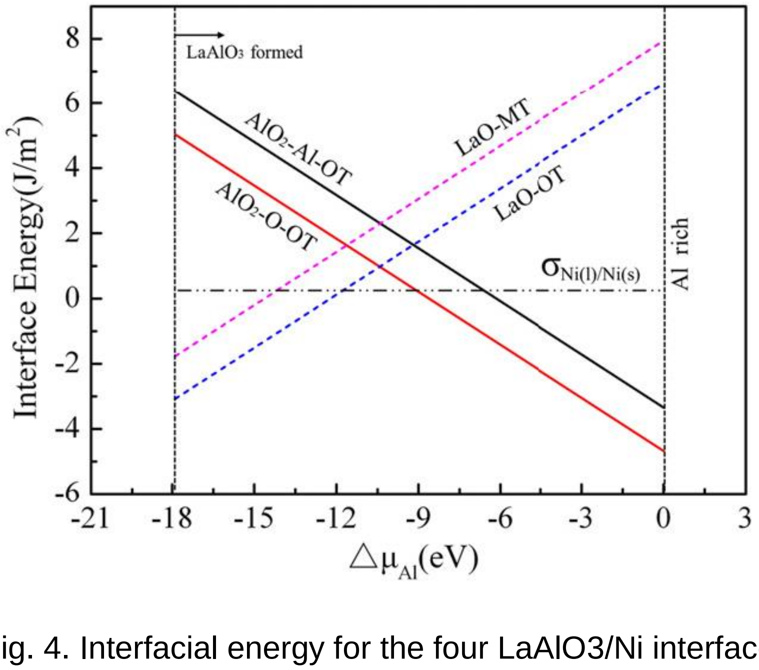

Fig. 4. Interfacial energy for the four LaAlO3/Ni interfaces as a function of ▵μAl.

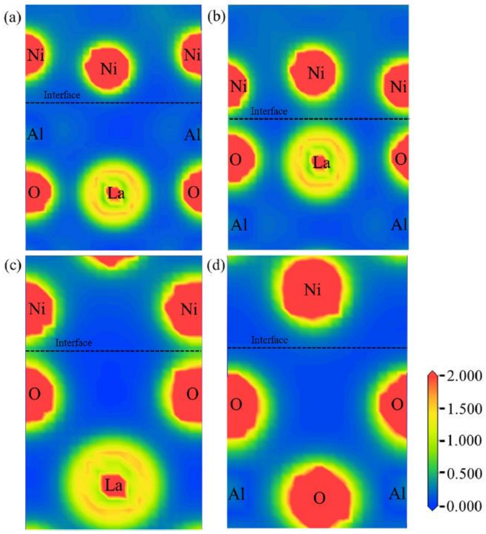

Fig. 5. Charge density for the four LaAlO3/Ni interfaces (e/Å3). (a) AlO2-Al-OT interface along (110) plane, (b) LaO-OT interface along (110) plane, (c) AlO2-O-OT interface along (200) plane, (d) LaO-MT interface along (100) plane.

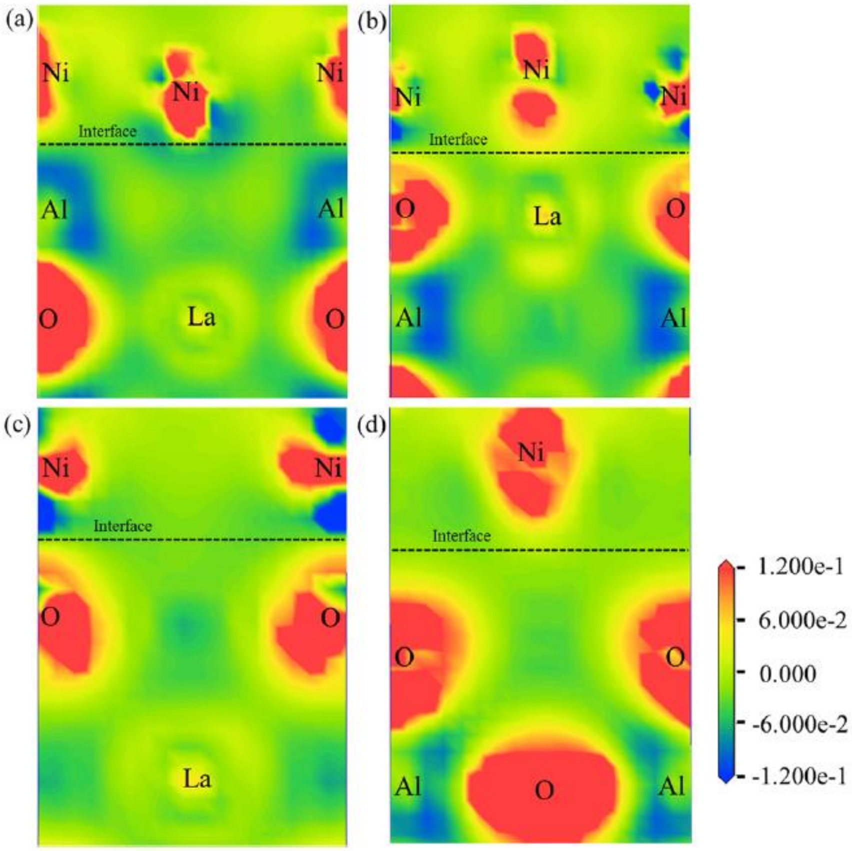

Fig. 6. Charge density difference for the four LaAlO3/Ni interfaces (e/Å3). (a) AlO2-Al-OT interface along (110) plane, (b) LaO-OT interface along (110) plane, (c) AlO2-O-OT interface along (200) plane, (d) LaO-MT interface along (100) plane.

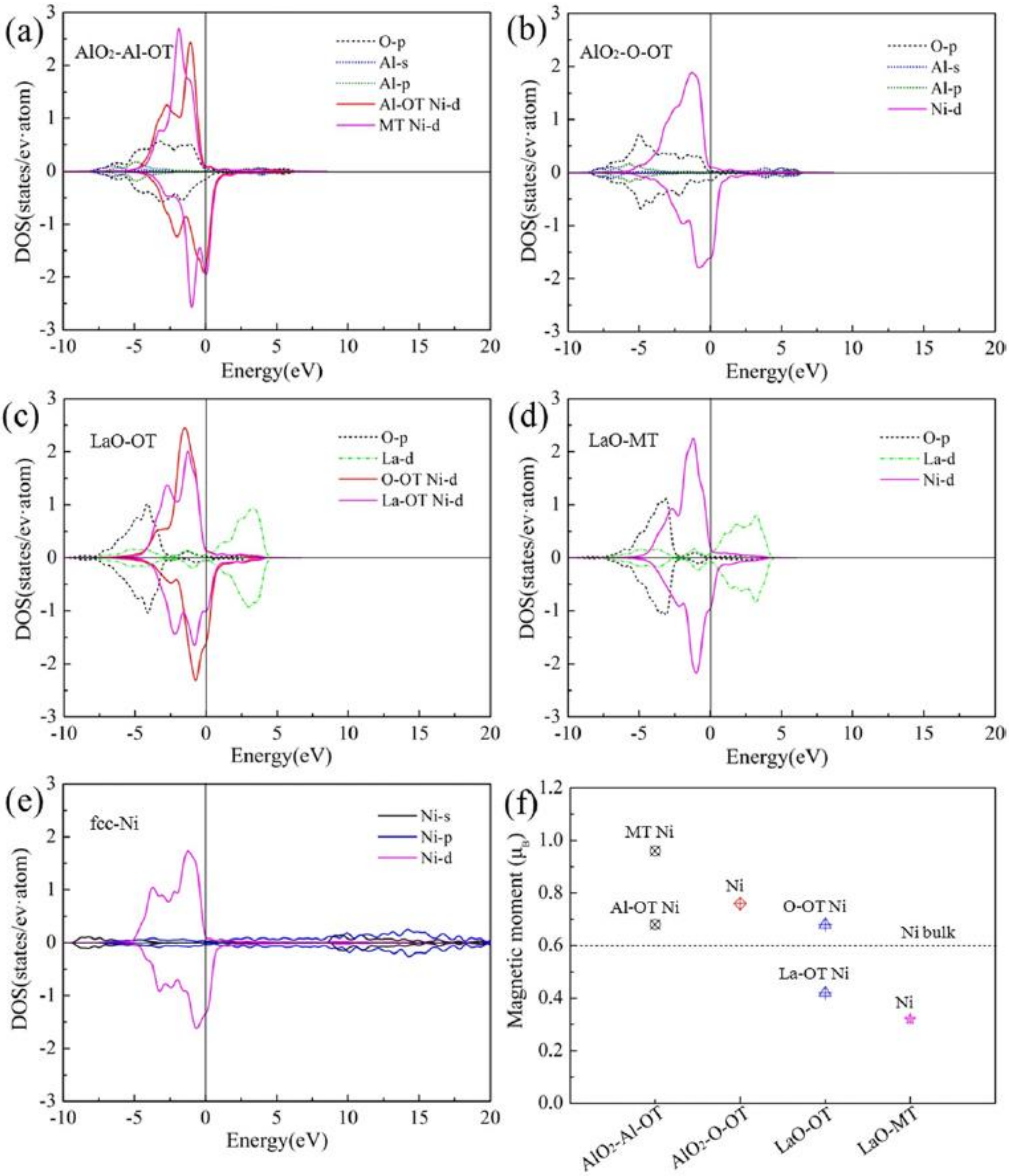

Fig. 7. Spin-polarized layer-projected partial DOS for atoms of (a) AlO2-Al-OT interface, (b) AlO2-O-OT interface, (c) LaO-OT interface, (d) LaO-MT interface, compared to (e) the bulk Ni partial DOS. (f) Magnetic moments per atom for corresponding Ni atoms of (a), (b), (c), (d) and (e).

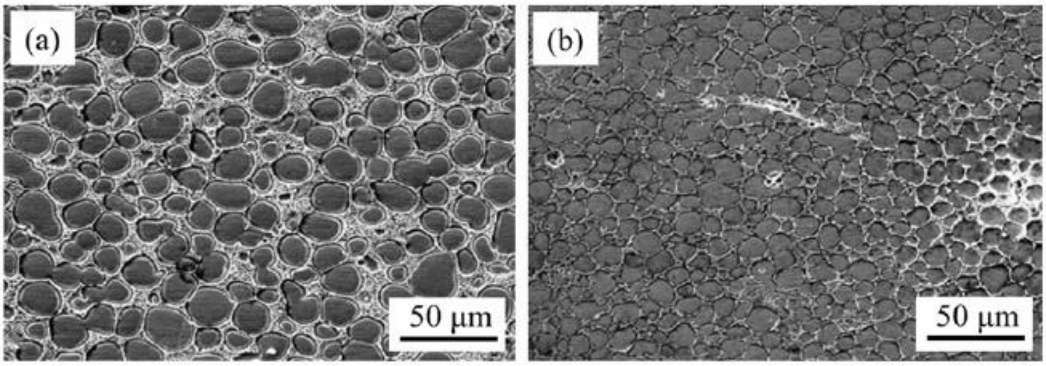

Fig. 8. Microstructure of (a) 0 wt.% La2O3 and (b) 1.2 wt.% La2O3 coatings [7].